Monthly Notices of the ROYAL ASTRONOMICAL SOCIETY
MNRAS **467,** 3500–3512 (2017) doi:10.1093/mnras/stw3297

Multicolour modelling of SN 2013dx associated with GRB 130702A*

A. A. Volnova,[1]† M. V. Pruzhinskaya,[2,3]† A. S. Pozanenko,[1,4,5] S. I. Blinnikov,[6,7,8] P. Yu. Minaev,[1] O. A. Burkhonov,[9] A. M. Chernenko,[1] Sh. A. Ehgamberdiev,[9] R. Inasaridze,[10] M. Jelinek,[11] G. A. Khorunzhev,[1] E. V. Klunko,[12] Yu. N. Krugly,[13] E. D. Mazaeva,[1] V. V. Rumyantsev[14] and A. E. Volvach[14]

[1]*Space Research Institute, 84/32 Profsoyuznaya Street, Moscow 117997, Russia*
[2]*Lomonosov Moscow State University, Sternberg Astronomical Institute, Universitetsky pr., 13, Moscow 119234, Russia*
[3]*Laboratoire de Physique Corpusculaire, Université Clermont Auvergne, Université Blaise Pascal, CNRS/IN2P3, Clermont-Ferrand, France*
[4]*National Research Nuclear University MEPhI (Moscow Engineering Physics Institute), 115409 Moscow, Russia*
[5]*Moscow Institute of Physics and Technology, 9 Institutskiy per., Dolgoprudny, Moscow Region, 141700, Russia*
[6]*Institute for Theoretical and Experimental Physics, Bolshaya Cheremushkinskaya ulitsa 25, 117218 Moscow, Russia*
[7]*All-Russia Research Institute of Automatics, Sushchevskaya ulitsa 22, 127055 Moscow, Russia*
[8]*Kavli Institute for the Physics and Mathematics of the Universe (WPI), The University of Tokyo Institutes for Advanced Study, University of Tokyo, 5-1-5 Kashiwanoha, Kashiwa 277-8583, Japan*
[9]*Ulugh Beg Astronomical Institute (UBAI) of the Uzbek Academy of Sciences, 33 Astronomicheskaya str., Tashkent 100052, Uzbekistan*
[10]*Kharadze Abastumani Astrophysical Observatory, Ilia State University, Kakutsa Cholokashvili Ave 3/5 Tbilisi 0162, Georgia*
[11]*Astronomical Institute of the Czech Academy of Sciences, Fričova 298, CZ-251 65 Ondřejov, Czech Republic*
[12]*Institute of Solar-Terrestrial Physics, Russian Academy of Sciences, Siderian Branch, 664033, Irkutsk PO Box 291, Lermontov st., 126a, Russia*
[13]*Kharkiv National University, Institute of Astronomy, 35 Sumska Str., Kharkiv UA-61022, Ukraine*
[14]*Crimean Astrophysical Observatory of the Russian Academy of Sciences, 298409, Crimea, Bakhchisaray Region, Nauchny, Russia*

Accepted 2016 December 15. Received 2016 December 14; in original form 2016 July 5

ABSTRACT

We present optical observations of SN 2013dx, related to the Fermi burst GRB 130702A, which occurred at red shift $z = 0.145$. It is the second-best sampled gamma-ray burst (GRB)/supernova (SN) after SN 1998bw. The observational light curves contain more than 280 data points in the *uBgrRiz* filters until 88 d after the burst, and the data were collected from our observational collaboration (Maidanak Observatory, Abastumani Observatory, Crimean Astrophysical Observatory, Mondy Observatory, National Observatory of Turkey and Observatorio del Roque de los Muchachos) and from the literature. We model numerically the multicolour light curves using the one-dimensional radiation hydrodynamical code STELLA, previously widely implemented for modelling typical non-GRB SNe. The best-fitting model has the following parameters: pre-SN star mass $M = 25\,M_\odot$; mass of the compact remnant $M_{CR} = 6\,M_\odot$; total energy of the outburst $E_{oburst} = 3.5 \times 10^{52}$ erg; pre-supernova star radius $R = 100\,R_\odot$; $M_{^{56}Ni} = 0.2\,M_\odot$, which is totally mixed through the ejecta; $M_O = 16.6\,M_\odot$; $M_{Si} = 1.2\,M_\odot$ and $M_{Fe} = 1.2\,M_\odot$, and the radiative efficiency of the SN is 0.1 per cent.

Key words: gamma-ray bursts: general – gamma-ray burst: individual: GRB 130702A – supernovae: general – supernovae: individual: SN 2013dx.

1 INTRODUCTION

The observational association between long-duration gamma-ray bursts (GRBs) and Type Ib/c supernovae (SNe) has been confirmed during last two decades, supporting the connection between GRBs and the death of massive stars (see, e.g. Hjorth & Bloom 2012). The first reliable association between a GRB and a SN was that of GRB 980425 with SN 1998bw, at a red shift $z = 0.0085$ (Galama et al. 1998; Iwamoto et al. 1998; Kulkarni et al. 1998). Since then about 40 SNe associated with GRBs have been discovered, and half of them are spectroscopically confirmed (e.g. SN 2003dh, Mazzali et al. 2003; SN 2006aj, Ferrero et al. 2007; SN 2010bh, Bufano et al. 2011; SN 2013cq, Perley et al. 2014; SN 2013fu, Cano et al. 2014, 2016).

To determine the physical properties of the SN explosion and/or of its progenitor (the mass of ^{56}Ni, the ejecta mass M_{ej}, the total

* Based on observations made with the Nordic Optical Telescope, operated on the island of La Palma jointly by Denmark, Finland, Iceland, Norway and Sweden, in the Spanish Observatorio del Roque de los Muchachos of the Instituto de Astrofisica de Canarias

† E-mail: alinusss@gmail.com (AAV); pruzhinskaya@gmail.com (MVP)

energy of the explosion $E_{\rm oburst}$ etc.) detailed photometrical and spectroscopic data are necessary. Due to the lack of observations, the most common way to estimate the physical parameters of GRB-SNe is to use the classical light curves (LCs) and spectra of well-studied SNe as templates (e.g. Cano 2013). Most often the multicolour and bolometric light curves of SN 1998bw and 2003dh are used. However, this empirical method of modelling is based on rather simple assumptions about SN explosions, initial conditions and evolution (Arnett 1982).

In this paper, we model the multicolour light curves of SN 2013dx, associated with GRB 130702A, using the code STELLA (Blinnikov et al. 1998, 2006). STELLA is a one-dimensional spherically symmetrical multi-group radiation hydrodynamics code that treats non-equilibrium radiative transfer according to the chemical composition and inner structure of a pre-SN star. The code has been used for light-curve modelling of different types of SNe (Ia, Blinnikov et al. 2006; Ib/Ic, Folatelli et al. 2006, Tauris et al. 2013; IIb, Blinnikov et al. 1998; IIn, Chugai et al. 2004; IIP, Baklanov, Blinnikov & Pavlyuk 2005, Tominaga et al. 2009). The assumptions about the SN outburst geometry are also simple, as in the empirical method, but the consideration of chemical abundances and the distribution of different chemical elements inside a pre-SN star allows one to calculate radiative transfer during the explosion and to build a more physically correct modelled light curve.

With the STELLA code, one can model many properties of the SN explosion. Spectra calculated for every specific time since the explosion allow one to model the multicolour light curves and photospheric velocities of the expanding SN envelope. The calculations take into account the distribution of the abundance of chemical elements in the envelope before the explosion, the interaction between the inner layers and the compact core. Another advantage of modelling is that it makes possible the investigation of a line-of-sight extinction by the circumburst medium by comparing modelled and observed light curves in various photometric filters.

The results from the STELLA code have been found to be in good agreement with those from other well-known hydrodynamic codes (e.g. Woosley et al. 2007; Kromer & Sim 2009; Sim et al. 2010; Kozyreva et al. 2017).

In Section 2, we present the observational data used for the modelling: we construct the detailed multicolour light curves using original observations and published data. In Section 3, we explain the process of SN light-curve extraction. In Section 4, we describe the modelling procedure with the STELLA code and present the properties of the model that matched best to the observed light curves of SN 2013dx. In Section 5, we discuss the remaining unresolved questions about the properties of both GRB 130702A and SN 2013dx.

2 OBSERVATIONS

2.1 Detection of GRB 130702A/SN 2013dx

GRB 130702A (= Fermi trigger 394416326) triggered the Gamma-ray Burst Monitor (GBM; Meegan et al. 2009) and was observed by the Large Area Telescope (LAT; Atwood et al. 2009) aboard the space observatory *Fermi* at 00:05:23.079 UT on 2013 July 2 (Cheung et al. 2013; Collazzi & Connaughton 2013). Hereafter, we consider this time as T_0, and all time intervals since the burst trigger are referred to as t. The burst had duration T_{90} (the time during which the cumulative counts increase from 5 to 95 per cent above background; Kouveliotou et al. 1993) of about 59 s in the GBM energy range 50–300 keV. *Fermi*/LAT detected more than five photons above 100 MeV up to $t = 2200$ s, and the highest energy photon is a 1.5 GeV event, which was observed 260 s after the GBM trigger (Cheung et al. 2013). The best LAT location found by Cheung et al. (2013) during on-ground analysis is $\alpha = 216.^\circ4$, $\delta = +15.^\circ8$ (J2000), with an error radius of $0.^\circ5$ (90 per cent containment, statistical error only). This position is 4° from the best GBM position ($\alpha = 218.^\circ81$, $\delta = +12.^\circ25$ with 1σ uncertainty of 4°), and $0.^\circ8$ from the position of the optical afterglow (OA) (Singer et al. 2013a).

The OA of GRB 130702A was discovered by the intermediate Palomar Transient Factory (Law et al. 2009; Rau et al. 2009) with the Palomar 48-inch Oschin telescope (P48) (Singer et al. 2013a,b). The source was labelled as iPTF13bxl with coordinates $\alpha = 14^{\rm h}29^{\rm m}14^{\rm s}.78$, $\delta = +15^\circ46'26''.4$ (J2000). The OA is located in the vicinity of two Sloan Digital Sky Survey (SDSS) sources: a bright galaxy SDSS J142914.57+154619.3 at a separation of $7''.6$, and a faint source SDSS J142914.75+154626.0 classified as a star in the catalogue, at a separation of $0''.6$. The latter was suggested to be a galaxy rather than a star, and to be the host galaxy of the burst in subsequent studies (Kelly et al. 2013; D'Elia et al. 2015, hereafter D15; Toy et al. 2016, hereafter T16).

The red shift of the OA was obtained based on the detection of Hα, O II and O III emission corresponding to $z = 0.145$ (Mulchaey et al. 2013a,b; D'Avanzo et al. 2013a). The red shift is consistent with that of one of the nearby bright galaxies SDSS J142914.57+154619.3 measured spectroscopically by Leloudas et al. (2013). This allowed Kelly et al. (2013) to suggest that the host galaxy of GRB 130702A may be a dwarf satellite of an adjacent massive spiral galaxy.

The emerging supernova SN 2013dx associated with GRB 130702A was discovered photometrically about 6 d after the burst trigger with the 2.5-m Nordic Optical Telescope (NOT) based on obvious brightening of the OA and a colour evolution that was unexpected for the decaying afterglow (Schulze et al. 2013). Later, the SN was confirmed spectroscopically (Cenko et al. 2013; D'Elia et al. 2013) and given the name SN 2013dx.

2.2 Observations in gamma-rays

The burst was also observed by Konus-*Wind* and had a fluence of $6.70^{+0.82}_{-0.80} \times 10^{-6}$ erg cm^{-2} in the 20–1200 keV energy range (Golenetskii et al. 2013). The gamma-ray emission of the burst was also detected by SPI-ACS/*INTEGRAL* and GRNS/*MESSENGER* (Hurley et al. 2013).

We analysed GRB 130702A's prompt emission in the gamma-ray domain using GBM/*Fermi* and SPI-ACS/*INTEGRAL* data. The light curve reveals two components in both SPI-ACS and GBM data. These components are the main episode of the emission with a duration of approximately 20 s and the extended emission with a duration of up to 650 s (Fig. 1). The duration of the burst was calculated in the energy range >80 keV using SPI-ACS data and found to be $T_{90} = 545 \pm 60$ s. The off-axis angle in SPI-ACS of GRB 130702A is 69°, which is close to optimal for detection.

The light curve of the main emission component in three energy channels of GBM is presented in Fig. 2. In the soft energy channel, 9–50 keV, the time profile has a smooth FRED-like shape.[1] The initial rising part of the second extended emission component is also visible, starting at approximately 15 s after the trigger. The extended emission in the hard energy channel is much weaker but it is also detectable up to 650 s after the trigger.

[1] FRED stands for fast rise and exponential decay – the common shape of GRB pulses.

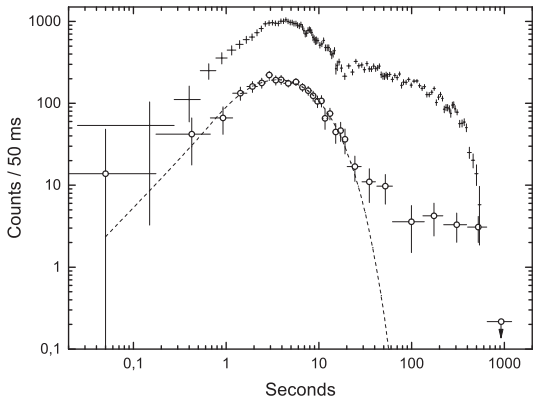

Figure 1. Background subtracted light curve of GRB 130702A from SPI-ACS/*INTEGRAL* (open circles, energy range 80–10 000 keV) and GBM/*Fermi* (crosses, energy range 9–900 keV). The dashed line represents the fit of the main emission component by an exponential model (Norris et al. 2005). The time in seconds since the burst prompt phase is presented. The flux in counts is presented per 50 ms time interval. The GBM/*Fermi* light curve is multiplied by a factor of 10 for clarity. The phase of the extended emission and the sharp cut-off at the end are clearly visible in both the GBM and SPI-ACS light curves.

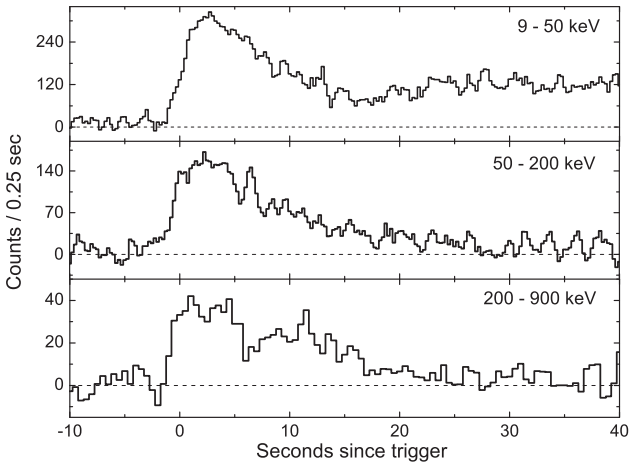

Figure 2. Background subtracted light curve of GRB 130702A in three energy bands (GBM/*Fermi*). The time resolution is 0.25 s for the 9–50 keV and 50–200 keV energy bands and 0.5 s for the 200–900 keV energy band. The horizontal axis is the time since the GBM trigger, while the vertical axis is the gamma-ray flux of each energy band.

The spectral lag analysis was performed on GBM/*Fermi* data for the main episode of emission in the time interval from −5 to 20 s after the trigger. The lag was calculated using the CCF method (Band 1997) between the channels 25–50 and 50–100 keV, and also between the channels 25–50 and 100–300 keV. In both cases, the spectral lag is almost negligible (0.3 ± 0.3 and 0.5 ± 0.3 s, respectively). According to Norris (2002), 80 per cent of long BATSE[2] GRBs have a lag less than 0.5 s between the channels 25–50 and 100–300 keV.

Spectral analysis was performed for the main episode in the time interval from −1.5 to 13 s after the trigger using `rmfit`[3] and data from the BGO_{01}, NaI_{06}, NaI_{07} and NaI_{08} detectors of GBM/*Fermi*.

[2] Burst and Transient Source Experiment, operated onboard the space Compton observatory in 1991–2000 Pačiesas 2004.
[3] http://fermi.gsfc.nasa.gov/ssc/data/analysis/rmfit/

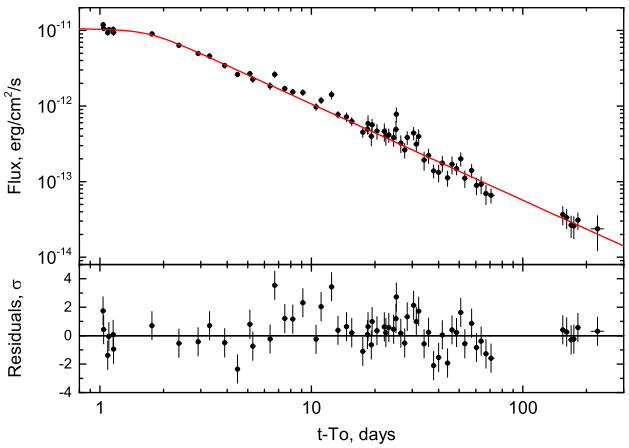

Figure 3. Upper panel: X-ray light curve in the range 0.3–10 keV, obtained by *Swift*/XRT (black circles). The data before $t = 20$ d were binned to give a better signal-to-noise ratio. The solid line is a BPL fit with the jet-break time $t_{\rm jb} = 1.7 \pm 0.2$ d, and the slope after the break $\alpha_{X,2} = -1.27 \pm 0.02$. Lower panel: Residuals of the fit.

The energy spectrum is fitted well by a single power-law model with index $\gamma = -1.78 \pm 0.02$. The fluence of the main emission episode in the 10–1000 keV energy range is $(6.17 \pm 0.22) \times 10^{-6}$ erg cm^{-2}.

2.3 *Swift*-XRT observations

The X-ray counterpart of GRB 130702A was observed by the X-Ray Telescope (XRT; Burrows et al. 2005) aboard the *Swift* space observatory (Gehrels et al. 2004) starting from 89.1 ks after the GBM trigger, i.e. $t = 1.03$ d (D'Avanzo et al. 2013b). The observations continued up to 225 d after the trigger.[4]

We downloaded the full X-ray light curve from the XRT Light Curve Repository (Evans et al. 2009) and fitted it with a broken power law (BPL; see, e.g. Beuermann et al. 1999) using the non-linear least squares method of Markwardt (2009). The best-fit parameters are the following: slope before the break $\alpha_{X,1} = 0.03 \pm 0.26$, slope after the break $\alpha_{X,2} = -1.27 \pm 0.02$ (Fig. 3, upper panel), jet-break time $t_{\rm jb} = 1.7 \pm 0.2$ d after the burst trigger, and sharpness of the break is fixed at 5, giving χ^2/DOF = 72/58. These parameters differ from those obtained by Singer et al. (2013b) because they used a restricted data set (the first 10 d instead of 225 d after the burst trigger) and fitted it with a single power law. We will assume that the afterglow light curve is achromatic after t_b between the X-ray and optical band-passes and use our best-fit X-ray light curve parameters to subtract the afterglow trend from the optical light curve of GRB 130702A.

The results of our fit and the known red shift allow us to estimate the isotropic-equivalent energy release in X-rays by integrating the obtained BPL function from 1 to 225 d after the trigger: $E_{{\rm iso},X} > 2.7 \times 10^{50}$ erg, which is a lower limit because of the absence of X-ray data before $t = 1.03$ d.

2.4 Optical follow-up

2.4.1 Our observations

We started to monitor the field of GRB 130702A with the 1.5-m AZT-22 telescope of Maidanak Astronomical Observatory on

[4] http://www.swift.ac.uk/xrt_curves/00032876/

2013 July 3, i.e. one and a half days after the *Fermi* trigger (Pozanenko et al. 2013). We took six frames in the *R* filter with exposures of 300 s each. The afterglow reported by Singer et al. (2013a) was clearly detected on a stacked frame. We continued the observations of the afterglow and rising SN taking several 300-s frames in the *R* band on July 4–12, 14–16, 18, 19, 21 and 23 and August 15, 18 and 28. We also took observations in the *B* band, taking frames with the same exposures on July 7, 10, 12 and 15.

The OA was observed by the 0.7-m AS-32 telescope of Abastumani Astrophysical Observatory by taking unfiltered images with exposures of 120 s on July 3, 4, 15 and 16. The 1-m Zeiss-1000 (Z-1000) telescope of the Simeiz branch of the Crimean Astrophysical Observatory took several 120-s frames of the OA and emerging SN in the *B* and *R* filters on July 13. The observations with this instrument were continued on July 15–16 only in the *R* filter, with the same exposures.

The 2.6-m Shajn telescope (ZTSh) of the Crimean Astrophysical Observatory observed the OA by taking a 1-h set of 60-s images in the *R* filter on July 5. The instrument also observed the decaying SN with 120-s frames taken on August 3 (*B* and *R*) and August 4 (only *R*).

The late phase of SN decay was observed by the 1.5-m Russian-Turkish telescope (RTT-150) at Tubitak observatory on August 28 (three frames of 300 s in the *R* band) and by the 2.5-m NOT at Roque de los Muchachos Observatory on September 27–28.

We observed the host galaxy on 2014 May 28 with ZTSh taking 81 images in the *R* filter and 54 images in the *B* filter with exposures of 60 s. However, the seeing in observations in the *R* filter was not good enough to separate clearly the host galaxy flux from that of the neighbouring big galaxy.

We also obtained images of the host galaxy on 2014 March 30 with the 1.5-m AZT-33IK telescope of the Sayan observatory (Mondy) in the *R* filter with a total exposure of 2 h. A log of all observations is presented in Table 1.

All our optical data were processed using the IRAF software package of the National Optical Astronomy Observatories (NOAO).[5] Standard image processing (bias, dark reduction and flat-fielding) was done using the task `ccdproc`. Some images were combined in sums using the tasks `imlintran` and `imcombine` to provide a better signal-to-noise ratio. The aperture photometry was done using the APPHOT subpackage, using an aperture radius of twice the full width at half-maximum that was measured for point sources on each night. The photometry is based on reference stars from SDSS-DR9 listed in Table 2 [*R* and *B* magnitudes are transformed from the *ugriz* system using Lupton's (2005) transformation equations[6]]. The unfiltered data from the Abastumani AS-32 telescope were calibrated using the same *R* magnitudes and the additional correction constant of +0.034 mag determined by the spectral properties of the AS-32 CCD and Johnson *R* filter and calculated using numerous optical observations of other GRB OAs.

All the data reported in Table 1 supersede the data previously published in GCN circulars (NN 14988, 14996, 15003, 15243).

[5] IRAF is the Image Reduction and Analysis Facility, a general purpose software system for the reduction and analysis of astronomical data. IRAF is written and supported by the NOAO in Tucson, Arizona. NOAO is operated by the Association of Universities for Research in Astronomy (AURA) Inc under a cooperative agreement with the National Science Foundation (http://iraf.noao.edu/).

[6] http://classic.sdss.org/dr6/algorithms/sdssUBVRITransform.html#Lupton2005

Table 1. Log of our observations. All magnitudes are in the AB system and are not corrected for Galactic extinction.

Date	UT start	T_0 +	Telescope	Filter	Magnitude
2013-07-03	17:38:18	1.7083	AZT-22	*R*	18.88 ± 0.04
2013-07-03	17:40:00	1.7554	AS-32	Clear	18.89 ± 0.03
2013-07-04	16:49:20	2.6743	AZT-22	*R*	19.43 ± 0.04
2013-07-04	19:32:52	2.7864	AS-32	Clear	19.33 ± 0.07
2013-07-05	16:25:11	3.6592	AZT-22	*R*	19.79 ± 0.02
2013-07-05	20:23:21	3.8377	ZTSh	*R*	19.86 ± 0.02
2013-07-06	16:20:12	4.6540	AZT-22	*R*	19.89 ± 0.03
2013-07-07	16:45:34	5.6716	AZT-22	*R*	20.01 ± 0.04
2013-07-08	16:49:14	6.6759	AZT-22	*R*	19.99 ± 0.05
2013-07-09	16:50:52	7.6770	AZT-22	*R*	19.91 ± 0.04
2013-07-10	17:31:29	8.6931	AZT-22	*R*	19.83 ± 0.03
2013-07-11	16:50:14	9.6644	AZT-22	*R*	19.80 ± 0.03
2013-07-12	17:19:13	10.6846	AZT-22	*R*	19.78 ± 0.03
2013-07-13	20:26:12	11.8144	Z-1000/CrAO	*R*	19.71 ± 0.04
2013-07-14	17:08:02	12.6768	AZT-22	*R*	19.70 ± 0.04
2013-07-15	16:44:09	13.6602	AZT-22	*R*	19.69 ± 0.04
2013-07-15	19:23:12	13.7853	AS-32	Clear	19.65 ± 0.06
2013-07-15	19:41:31	13.7988	Z-1000/CrAO	*R*	19.69 ± 0.04
2013-07-16	17:25:47	14.6891	AZT-22	*R*	19.65 ± 0.05
2013-07-16	21:08:17	14.8524	Z-1000/CrAO	*R*	19.68 ± 0.07
2013-07-16	21:30:57	14.8678	AS-32	Clear	19.58 ± 0.07
2013-07-18	16:56:54	16.6691	AZT-22	*R*	19.62 ± 0.04
2013-07-19	16:54:58	17.6677	AZT-22	*R*	19.74 ± 0.04
2013-07-21	17:29:40	19.6918	AZT-22	*R*	19.72 ± 0.05
2013-07-23	17:23:24	21.6875	AZT-22	*R*	19.75 ± 0.05
2013-08-03	19:40:37	32.7930	ZTSh	*R*	20.70 ± 0.03
2013-08-04	18:55:51	33.7762	ZTSh	*R*	20.71 ± 0.03
2013-08-15	11:43:16	44.4624	AZT-22	*R*	21.13 ± 0.12
2013-08-18	11:38:02	47.4688	AZT-22	*R*	21.44 ± 0.11
2013-08-28	11:48:54	57.4622	AZT-22	*R*	21.77 ± 0.07
2013-08-28	18:39:39	57.7404	RTT-150	*R*	21.83 ± 0.14
2013-09-27/28	20:02:28	88.3032	NOT	*R*	22.40 ± 0.09
2014-03-30	18:48:51	271.7885	AZT-33IK	*R*	22.66 ± 0.10
2014-05-28	18:59:39	361.7866	ZTSh	*R*	22.71 ± 0.08
2013-07-07	17:18:43	5.6947	AZT-22	*B*	20.56 ± 0.08
2013-07-10	16:40:59	8.6581	AZT-22	*B*	20.46 ± 0.08
2013-07-12	17:52:31	10.7077	AZT-22	*B*	20.65 ± 0.07
2013-07-13	20:39:28	11.8607	Z-1000/CrAO	*B*	20.51 ± 0.25
2013-07-14	17:29:51	13.6920	AZT-22	*B*	20.64 ± 0.06
2013-08-03	18:47:33	32.7642	ZTSh	*B*	22.29 ± 0.07
2014-05-28	20:35:56	361.8417	ZTSh	*B*	23.54 ± 0.20

2.4.2 *Data from other sources*

We collected all available data on GRB 130702A and SN 2013dx observations published up to now. We took 87 photometrical points from D15 in the *uUgri* filters and 192 points from T16 in the $g'r'i'z'$ filters. We added six points from Singer et al. (2013b) in the *B* filter but due to the lack of numerical data in explicit form, we estimated the corresponding values based on fig. 3 of Singer et al. (2013b) with the magnitude uncertainties $0\overset{m}{.}1$.

We also adopted the host galaxy magnitudes obtained by T16 in the $u'g'r'i'z'$ filters at $t = 632$ d and in the *R* filter at $t = 330$ d after the trigger.

We converted *U* values from D15 and our *R* magnitudes from the Vega to the AB system and then to *u* and *r*, respectively, using methods from Blanton & Roweis (2007). We also converted all magnitudes used for construction of light curves from the $u'g'r'i'z'$ to the *ugriz* system using SDSS photometric equations.[7] The observed multicolour light curves of the GRB 130702A optical counterpart are presented in Fig. 4.

[7] http://classic.sdss.org/dr7/algorithms/jeg_photometric_eq_dr1.html

Table 2. Reference stars from SDSS-DR9 used for the photometry. *R* and *B* magnitudes were obtained from *ugriz* data using Lupton's 2005 transformation equations.

N	SDSS ID	*u*	*g*	*r*	*i*	*z*	*R*	*B*
1	J142915.86+154510.0	17.968 (0.012)	16.721 (0.004)	16.228 (0.004)	16.029 (0.004)	15.963 (0.007)	16.033 (0.013)	17.095 (0.013)
2	J142911.60+154535.2	19.808 (0.034)	17.303 (0.005)	15.920 (0.004)	15.261 (0.004)	14.933 (0.005)	15.576 (0.013)	17.935 (0.035)
3	J142922.06+154652.2	20.070 (0.043)	19.030 (0.009)	18.715 (0.009)	18.607 (0.011)	18.562 (0.030)	18.550 (0.020)	19.356 (0.045)
4	J142911.64+154807.2	18.994 (0.022)	17.390 (0.005)	16.800 (0.004)	16.565 (0.004)	16.433 (0.008)	16.591 (0.013)	17.813 (0.023)
5	J142923.79+154823.4	21.009 (0.084)	18.575 (0.007)	17.627 (0.006)	17.288 (0.006)	17.109 (0.011)	17.370 (0.015)	19.132 (0.085)

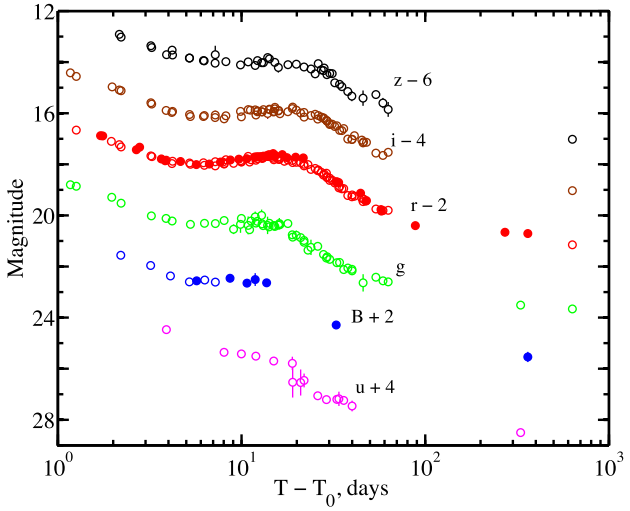

Figure 4. Observed multicolour light curves of SN 2013dx connected with GRB 130702A. Filled and open circles depict the data presented in this work and collected from the literature, respectively (see Section 2.4.2). The SN phenomenon is clearly seen in every filter. Galactic extinction is not taken into account.

2.5 Radio observations

The afterglow of GRB 130702A was observed at millimetre wavelengths with the Combined Array for Research in Millimeter Astronomy (CARMA) on 2013 July 4, i.e. 2 d after the trigger, at a frequency of 93 GHz (a wavelength of 3 mm) (Perley & Kasliwal 2013). A source coincident with the optical counterpart was discovered with a flux density ∼2 mJy.

The afterglow was also observed by the Westerbork Synthesis Radio Telescope at 4.9 GHz 2.56–3.05 d after the burst (van der Horst 2013). A radio source with a flux density of 1.23 ± 0.04 mJy was detected at the position of the optical counterpart. The radio counterpart was also observed with the Karl G. Jansky Very Large Array in the *C* band 2.29 d after the GBM trigger (Corsi, Perley & Cenko 2013). The radio source was detected with a flux density of 1.49 mJy at 5.1 GHz and 1.60 mJy at 7.1 GHz.

We observed the position of the radio afterglow using the 22-m radio telescope RT-22 of the Crimean Astrophysical Observatory at 36 GHz on 2013 July 5 and 6, i.e. 3.69 and 4.68 d after the trigger. At the position of the afterglow, we obtained 2σ upper limits of 0.6 and 0.5 mJy, respectively.

A summary of the GRB 130702A afterglow properties is collected in Table 3.

2.6 Host galaxy

Kelly et al. (2013) reported that GRB 130702A occurred in a dwarf satellite of a massive galaxy at a red shift $z = 0.145$ and provided some physical properties of the galaxy using a spectral energy distribution (SED) based on the SDSS *ugriz* photometry. As input parameters, we took the $u'g'r'i'z'JK_s$ magnitudes of the host galaxy from T16 and the *B* magnitude from ZTSh (see Table 1). We fixed the red shift and fitted the SED of the galaxy using the Le Phare software package (Arnouts et al. 1999; Ilbert et al. 2006). We used the pegase2 population synthesis model library (Fiok & Rocca-Volmerange 1997) to obtain the best-fitting SED and the main physical parameters of the galaxy: age, mass and star formation rate (SFR). The apparent magnitudes used for the fitting are listed in Table 4.

The host galaxy of GRB 130702A (χ^2/DOF=2.9/8) is fitted by the SED of an irregular dwarf galaxy with an age of 4.3×10^9 yr and

Table 3. Summary of GRB 130702A and its afterglow properties.

Discovered by	GBM/*Fermi*
T_0	00:05:23.079 UT on July 2, 2013
α, δ (GBM)	218.°81, +12.°25, 4° radius (Collazzi & Connaughton 2013)
α, δ (LAT)	216.°4, +15.°8, 0.°5 radius (Cheung et al. 2013)
T_{90} (GBM)	59 s (Collazzi & Connaughton 2013)
T_{90} (SPI-ACS)	545 ± 60 s
Highest energy	1.5 GeV (Cheung et al. 2013)
z	0.145 (Mulchaey et al. 2013a,b; D'Avanzo et al. 2013a)
$t_{\rm jb}^{o}$	1.17 ± 0.09 d (Singer et al. 2013b)
$t_{\rm jb}^{X}$	1.7 ± 0.2 d
α_2	1.27 ± 0.02
$E_{{\rm iso},\gamma}$	$(6.6 \pm 0.4) \times 10^{50}$ erg
$E_{{\rm iso},X}$	$>2.7 \times 10^{50}$ erg

Note. ^{o}indicates obtained using optical data; ^{X}indicates obtained using X-ray data.

Table 4. A summary of the GRB 130702A host galaxy properties. The magnitudes are in the AB system and are corrected for the expected Galactic foreground extinction.

Type	Irregular dwarf
M_r	-16.2^m
$u'_{\rm host}$	24.32 ± 0.21 (T16)
$B_{\rm host}$	23.39 ± 0.20
$g'_{\rm host}$	23.52 ± 0.06 (T16)
$r'_{\rm host}$	23.05 ± 0.06 (T16)
$R_{\rm host}$	23.17 ± 0.06 (T16)
$i'_{\rm host}$	22.96 ± 0.09 (T16)
$z'_{\rm host}$	22.97 ± 0.18 (T16)
$J_{\rm host}$	23.15 ± 0.48 (T16)
$K_{s,{\rm host}}$	>22.28 (T16)
Age	4.3×10^9 yr
$M_{\rm host}$	1.3×10^8 M$_\odot$
$A_V^{\rm host}$	∼0
SFR$_{\rm host}$	0.05 M$_\odot$ yr^{-1}

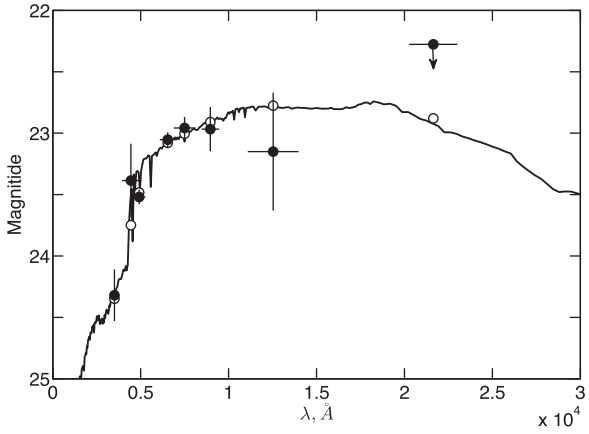

Figure 5. SED (line) of the host galaxy of GRB 130702A fitted by Le Phare with a fixed red shift. Filled circles depict the data points in the $u'Bg'r'i'z'JK_s$ filters, taken from T16 and from ZTSh observations. Open circles show the model magnitudes for each filter.

a mass of $M_{\rm host} = 1.3 \times 10^8\,{\rm M}_\odot$, which is slightly higher than the mass reported by Kelly et al. (2013). We also obtained negligible mean extinction in the host $A_V^{\rm host} = 0$ with the best extinction law of the Small Magellanic Cloud (Prévot et al. 1984) and a star formation rate ${\rm SFR}_{\rm host} = 0.05\,{\rm M}_\odot\ {\rm yr}^{-1}$. The two latter results are in a good agreement with those of previous studies (Kelly et al. 2013). The best-fitting SED of the host galaxy is shown in Fig. 5. A summary of the host galaxy properties are collected in Table 4.

3 SN LIGHT CURVE

To construct the light curve of a SN associated with a GRB, one needs to take into account the contribution from the GRB OA, the GRB host galaxy and light extinction in the Galaxy and in the host galaxy.

First, all photometrical data of GRB 130702A were corrected for Galactic extinction using the extinction maps from Schlafly & Finkbeiner (2011) with $E(B-V) = 0.038$.

Secondly, the contribution of the host galaxy was eliminated by flux subtraction. We used data from T16 for the *ugriz* filters (see Section 2.4.2). For the *B* filter, we used the value calculated via the Lupton (2005) transformation equations from *ugr* values of T16.

To distinguish the OA from the SN, we considered an approximation with the broken power-law slope obtained from the X-ray afterglow light curve (see Section 2.3) and assumed that the decay of the afterglow is achromatic from the X-ray to optical domains after the jet-break (see section 4.1 in T16), and thus, we fitted the optical data obtained between t_b and $t = 4$ d after the trigger with a single power law with fixed $\alpha_X = -1.27$ (see Section 2.3) and then subtracted the calculated flux from all photometrical points.

T16 estimated the host extinction as $A_V = 0.13 \pm 0.23$ by fitting the SED of the galaxy with a simple power-law model. This value is consistent with zero within the 1σ confidence interval, moreover, our modelling of the host galaxy SED showed that the mean host extinction is negligible, so we assumed $A_V^{\rm host} = 0$ and did not to take it into account in further modelling.

Finally, we converted all values to AB magnitudes and constructed the optical light curves of SN 2013dx, which are shown in Fig. 6(a). We also constructed the quasi-bolometric light curve of the SN in the AB photometric system by taking the sum of the fluxes in the *ugriz* filters. We used the code from Ishida & de Souza (2013) and Ishida, Abdalla & de Souza (2014),[8] which adapts Gaussian processes for interpolating the light curves. Since the data coverage in the *u* filter is less than the others, we had to interpolate the *u* light curve between 20 and 35 d and to extrapolate after $t = 35$ d. We assumed that the $u - g$ colour corresponding to the last day of observations in the *u* filter remains unchanged up to $t = 60$ d. The quasi-bolometric light curve is also shown in Fig. 6(a).

4 MODELLING OF THE SN LIGHT CURVE

4.1 Modelling

The numerical multicolour light-curve calculations for SN 2013dx were performed with the one-dimensional multi-frequency radiation hydrodynamics code STELLA (Blinnikov et al. 1998, 2006). In the current calculations, we adopted 100 zones for the Lagrangian coordinate and 130 frequency bins. As input parameters, we varied the pre-SN star mass *M* and radius *R*, the energy of the outburst $E_{\rm oburst}$, the mass of synthesized nickel $M_{^{56}{\rm Ni}}$, the mass of the resulting compact remnant $M_{\rm CR}$, and the initial distribution of chemical elements in the pre-SN star.

The mass $M_{\rm CR}$ in the central part of a pre-SN star with a fixed radius (which is much less than the outer radius of the star) is treated as a point-like source of gravity that has a non-negligible influence on the expansion of the innermost layers of SN ejecta. The explosion is initiated by putting thermal energy into the innermost layers. The ejecta of a SN has the same chemical composition as a pre-SN star except for ^{56}Ni, because we do not follow the explosive nucleosynthesis. ^{56}Ni can be put in the centre of SN ejecta in the calculations and as well as it can be spread out within any region.

The mass and radius of the pre-SN star for the model that offers the best agreement with the observations of SN 2013dx are $M = 25\,{\rm M}_\odot$ and $R = 100\,{\rm R}_\odot$. The resulting energy of the explosion is $E_{\rm oburst} = 3.5 \times 10^{52}$ erg. A part of the outburst energy goes into radiation from the far-IR to the extreme UV (in the range from 6.3×10^{13} Hz or 4.8 μm to 1.7×10^{16} Hz or 70 eV), i.e. the bolometric energy $E_{\rm bol}$ in the time interval 126 d after the trigger was 3.1×10^{49} erg. The $0.2\,{\rm M}_\odot$ of ^{56}Ni is totally mixed through the ejecta. The central region becomes a black hole with $M_{\rm CR} = 6\,{\rm M}_\odot$. The parameters $E_{\rm oburst}$ and $M_{^{56}{\rm Ni}}$ were adopted from D15. The rest of the parameters were picked by the model to match the observed light curve better.

Fig. 6(a) compares the optical (*ugriz* and *B*) light curves of the model with the observations of SN 2013dx. From the observational data in the *ugriz* filters, the quasi-bolometric light curve was also derived and compared with the modelled one. The quasi-bolometric light curve of the SN in the AB photometric system is obtained as a sum of the fluxes in the *ugriz* filters. To match better the observational and modelled light curves, a global time offset (3 d), i.e. a simultaneous time-shift of the modelled light curves relative to T_0, has been applied. Fig. 6(a) shows that the modelled light curves match adequately the observations from the *z* to the *g* filters, especially for the quasi-bolometric one. However, in the blue filters (*B* and *u*), the model and observations disagree. We discuss the possible nature of this behaviour in Section 5. Also, we obtained the value of $t_{\rm peak}$, which is the time of the maximum for the quasi-bolometric modelled light curve relative to the trigger time T_0.

[8] https://github.com/emilleishida/snclass

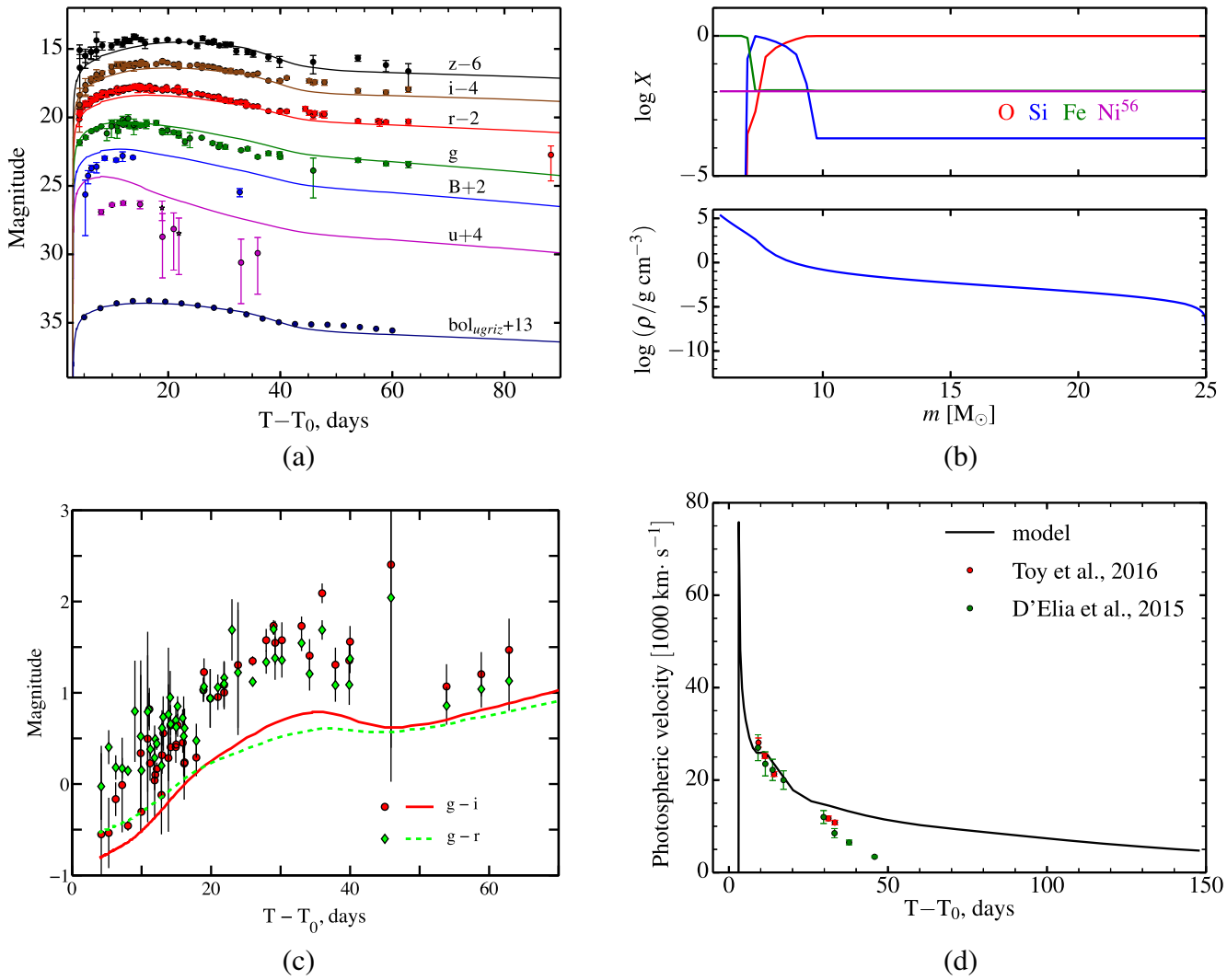

Figure 6. (a) Multicolour light curves of SN 2013dx. The Galactic extinction, the flux from the host galaxy and the OA contribution are excluded. Solid lines show the best model of the SN light curve obtained by STELLA (see Section 4). The quasi-bolometric light curve of the SN in the AB photometric system obtained as a sum of the fluxes in the *ugriz* filters is marked as bol_{ugriz}. The data and model are in the observer frame. (b) Mass fractions of O, Si, Fe and ^{56}Ni in the ejecta and density profile for the optimal pre-SN star model with respect to the interior mass. The central region of 6 $M_\odot$ is taken away. (c) Colour evolution of SN 2013dx. Points and lines show the variation of colour indices $g - i$ (red circles and red solid line) and $g - r$ (green diamonds and green dashed line) with time, for the observations and an optimal model. (d) Evolution of photospheric velocities of SN 2013dx measured via observations (points) and calculated from the modelling (solid line). The plot is in the observer frame.

The distribution of chemical elements and the density profile for a pre-SN star are shown in Fig. 6(b). Note that the model shows a total absence of hydrogen and helium in the pre-SN star composition, which is common for Type Ic SNe (Filippenko 1997).

In Fig. 6(c), we plot the colour evolution of the SN, and Fig. 6(d) shows the observer-frame photospheric velocities in comparison with observational data obtained via spectroscopy by D15 and T16. The model evolution of the photospheric velocities is in good agreement with direct observations during the first ∼30 d after the explosion. A summary of the SN 2013dx parameters is collected in Table 5. It also compares the parameters of the SN obtained by other studies.

Following the description of the SN explosion parameters in T16, we performed LC modelling adopting $M_{^{56}\mathrm{Ni}} = 0.37\ \mathrm{M}_\odot$ (located in the centre of the explosion and no mixing), $E_\mathrm{K} = 8.2 \times 10^{51}$ erg and $M_\mathrm{ej} = 3.1\ \mathrm{M}_\odot$. In the current model, we assumed, following

Table 5. Summary of the SN 2013dx parameters obtained by STELLA in comparison with those of D15 and T16. All masses are in $\mathrm{M}_\odot$.

Parameter	STELLA model	D15	T16
M	25	∼25–30[a]	–
M_CR	6	–	–
E_oburst	3.5×10^{52} erg	$\sim 3.5 \times 10^{52}$ erg	$(8.2 \pm 0.4) \times 10^{51}$ erg
M_ej	19	∼7	3.1 ± 0.1
R	$100\,\mathrm{R}_\odot$	–	–
$M_{^{56}\mathrm{Ni}}$	0.2, totally mixed	∼0.2	0.37 ± 0.01
M_O	16.6	–	–
M_Si	1.2	–	–
M_Fe	1.2	–	–
E_bol	3.1×10^{49} erg	–	–
t_peak	14.35 d[b]	15 ± 1 d[c]	13.2 ± 0.3 d[c]

[a]Mass of the progenitor on the main sequence; [b]on the bolometric light curve; [c]on the light curve in the *r* filter.

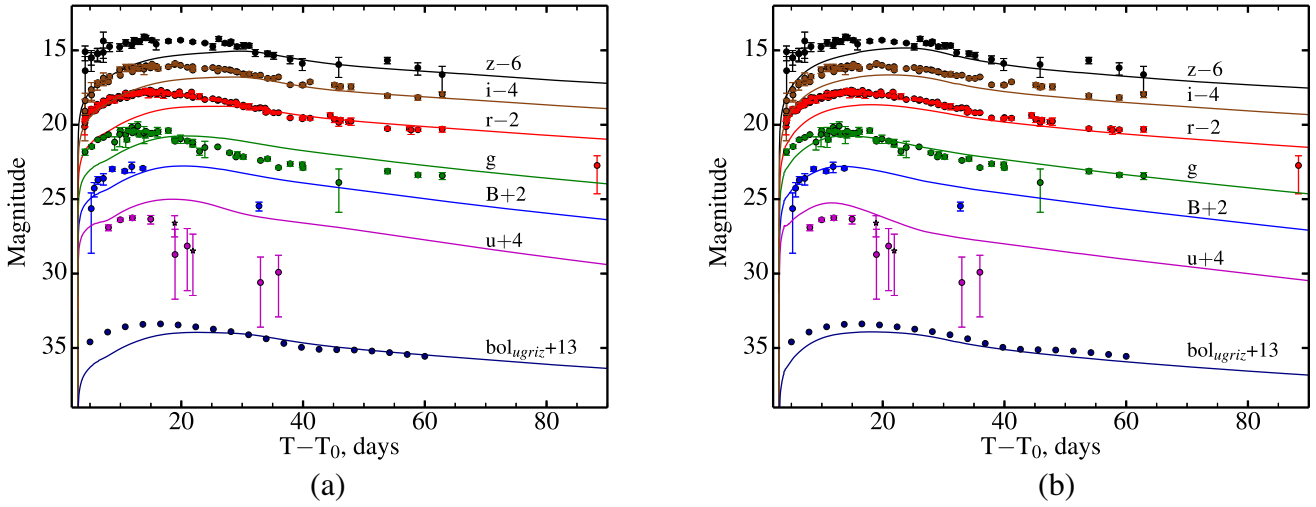

Figure 7. The result of modelling (lines) the observed light curves of SN 2013dx (points) with $M_{\rm ej} = 3.1\ {\rm M}_\odot$, $M_{^{56}{\rm Ni}} = 0.37\ {\rm M}_\odot$ and $E_K = 8.2 \times 10^{51}$ erg corresponding to T16. Two different distributions of ^{56}Ni in the ejecta are considered: (a) totally mixed and (b) not mixed. The quasi-bolometric light curve of the SN in the AB photometric system obtained as a sum of the fluxes in the *ugriz* filters is marked as bol$_{ugriz}$.

T16, that there is no compact object at all, i.e. no gravitational centre that affects the expansion of the innermost layers. Since in T16 it is written that the initial radius before the explosion is small, we put $R = 10\,{\rm R}_\odot$. Fig. 7(a) compares SN 2013dx observations with the STELLA model for the T16 SN parameters. In the early phases, the modelled light curves lie below the observational ones in all filters. Starting from ∼30 d after the explosion, *z*, *i*, *r* and the quasi-bolometric modelled light curves fit the observational data well. We also made a model keeping absolutely the same parameters as in T16 but with the nickel totally mixed in the ejecta as in our optimal model. The nickel mixing partly improved the increasing part of the modelled light curves, making them a bit more consistent with observations (see Fig. 7b). The global time offset (3 d) has been applied to all light curves modelled.

4.2 Influence of different initial parameters

In this section, we consider the dependence of the quasi-bolometric light curve on an input physical parameter of the model while the others remain fixed. We varied the mass M and the radius R of the pre-SN star, the mass of synthesized ^{56}Ni and the energy of the burst $E_{\rm oburst}$. Plots comparing the observational quasi-bolometric light curves are presented in Fig. 8.

Figs 8(a), (b) and (c) demonstrate that the ejecta mass affects the descending part of the light curve, the dependence of the radius is stronger at the domes of the light curve, however, the tail is mainly determined by the ^{56}Ni abundance. The models are brighter for higher ejecta or ^{56}Ni mass, and larger radius. Decreasing the compact remnant mass gives a wider maximum of the light curve. In Figs 8(b), (c) and (d), we also present the models with the same amount of ^{56}Ni as our optimal model (0.2 M$_\odot$) but with and without mixing through the ejecta. When ^{56}Ni is mixed, the light-curve maximum is brighter. Moreover, the gamma photons from radioactive decay are not trapped inside an envelope and do not heat the ejecta. Therefore, the photosphere goes faster to the centre and the SNe becomes dimmer on the tail.

Decreasing the outburst energy increases the diffusion time of gamma photons from radioactive decay. This manifests itself as a widening of the light curve, moreover, the diminution of the decline rate occurs later (see Fig. 8d). Approximate limits of the main model parameters can be derived based on Fig. 8. The pre-SN star mass and radius vary in the range 23–27 M$_\odot$ and 75–125 R$_\odot$, respectively, the ^{56}Ni mass lies between 0.15 and 0.25 M$_\odot$, and the explosion energy $E_{\rm oburst}$ is in the range (30–40) $\times\ 10^{51}$ erg.

5 DISCUSSION

5.1 The nature of the extended emission of GRB 130702A

In Section 2.2, we mentioned the extended emission of GRB 130702A observed in gamma-rays, and now we would like to discuss its possible nature.

The main component in the SPI-ACS data has a smooth shape, which can be fitted with an exponential function (Norris et al. 2005). The extended emission in both GBM and SPI-ACS data looks like a plateau with a cut-off at about 650 s after the trigger. This component could be connected with the activity of a rapidly spinning magnetar, which initially formed during the core-collapse stage. It is clear that the mass of the compact remnant 6 M$_\odot$ (see Section 4) is more than the Oppenheimer–Volkoff limit, and the cut-off may be a manifestation of a delayed collapse into a black hole of a spin-down magnetar (Vietri & Stella 1998; Lyons et al. 2010), which has already been proposed to explain the extended emission phase of some GRBs (e.g. De Pasquale et al. 2016).

Alternatively, the source of the prompt emission could be a neutrino-heated jet (MacFadyen & Woosley 1999). Later, if the accretion rate is high enough, the activation of a Blandford–Znajek jet (Komissarov & Barkov 2009) could be the source of the high-energy extended emission (Barkov & Pozanenko 2011). The emission cut-off could be explained by a rapid decrease of the accretion rate. The latter scenario is less plausible because of the high radius of a pre-SN star and consequently the large size of the accretion disc. A detailed analysis of the extended emission of GRB 130702A will be presented elsewhere (Minaev et al., in preparation).

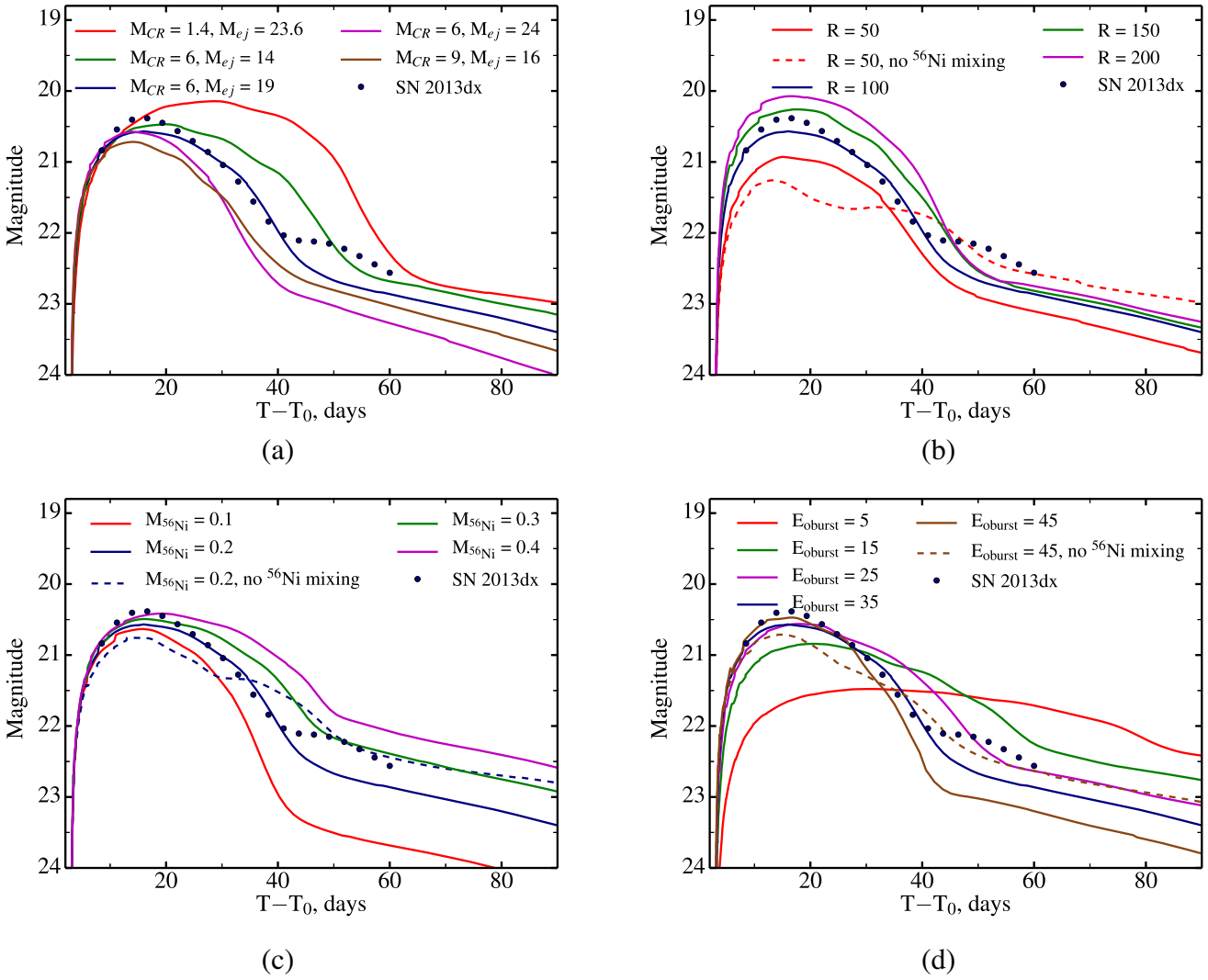

Figure 8. The dependence of the quasi-bolometric light curve (*ugriz* filters) on the different parameters of the optimal model (dark blue curve): (a) the mass of the pre-SN star and its distribution between the ejecta and the compact remnant (here and in other panels masses are in units of Solar mass), (b) the radius of the pre-SN star in units of Solar radius, (c) the mass of the synthesized ^{56}Ni, (d) the energy of the outburst in units of 10^{51} erg. Filled circles show the observational quasi-bolometric light curve of SN 2013dx. ^{56}Ni is totally mixed through the ejecta for all models presented except the models shown with a dashed line.

5.2 The Amati relation

Assuming a power-law model to be valid down to 1 keV (see Section 2.1), we found the fluence of the burst to be $(1.31 \pm 0.08) \times 10^{-5}$ erg cm^{-2} in the energy range 1–10 000 keV. Assuming $z = 0.145$ and a standard cosmology model with $H_0 = 69.6\,\mathrm{km\,s^{-1}}$ Mpc^{-1}, $\Omega_M = 0.286$ and $\Omega_\Lambda = 0.714$ (Wright 2006; Bennett et al. 2014), the isotropic energy release in 1–10 000 keV is $E_{\mathrm{iso},\gamma} = (6.6 \pm 0.4) \times 10^{50}$ erg in the GRB rest frame.

Almost all long GRBs follow relation $E_{\mathrm{peak}} \times (1 + z) - E_{\mathrm{iso}}$ (Amati et al. 2002). If we assume that GRB 130702A also follows the Amati relation, then its $E_{\mathrm{peak}} \times (1 + z)$ parameter should be within 7–50 keV ($\pm 2\sigma$ coincidence level). However, the energy spectrum of GRB 130702A is fitted well by a simple power-law model with index $\gamma = -1.78 \pm 0.02$ and does not show the presence of a spectral break in energy range 10–15 000 keV. The value of the spectral index is typical for β of a Band function (Band et al. 1993) and may indicate that E_{peak} is less than the lower limit of the analysed energy range: the median values of spectral parameters obtained for GBM bursts are shown in tables 3 and 4 of Gruber et al. (2014). Under this assumption, we estimate the upper limit of E_{peak} to be approximately 10 keV. In this case, GRB 130702A will follow the Amati relation. A similar result was also obtained by Amati et al. (2013).

5.3 Late X-ray light curve

In Section 2.3, we fitted the X-ray light curve of GRB 130702A with a BPL. There is an enhancement of the flux in the residuals plot (see lower panel of Fig. 3). The flux of the enhancement, integrated in the time interval 5–15 d after the trigger, is $F^+ = (2.4 \pm 0.6) \times 10^{-12}$ erg cm^{-2} s^{-1}, which is equivalent to the luminosity $L^+_{4\pi} = (1.4 \pm 0.3) \times 10^{43}$ erg s^{-1}. Here we use the luminosity distance $D_L = 692$ Mpc corresponding to $z = 0.145$. We cannot distinguish whether this is related to flare activity of the GRB afterglow

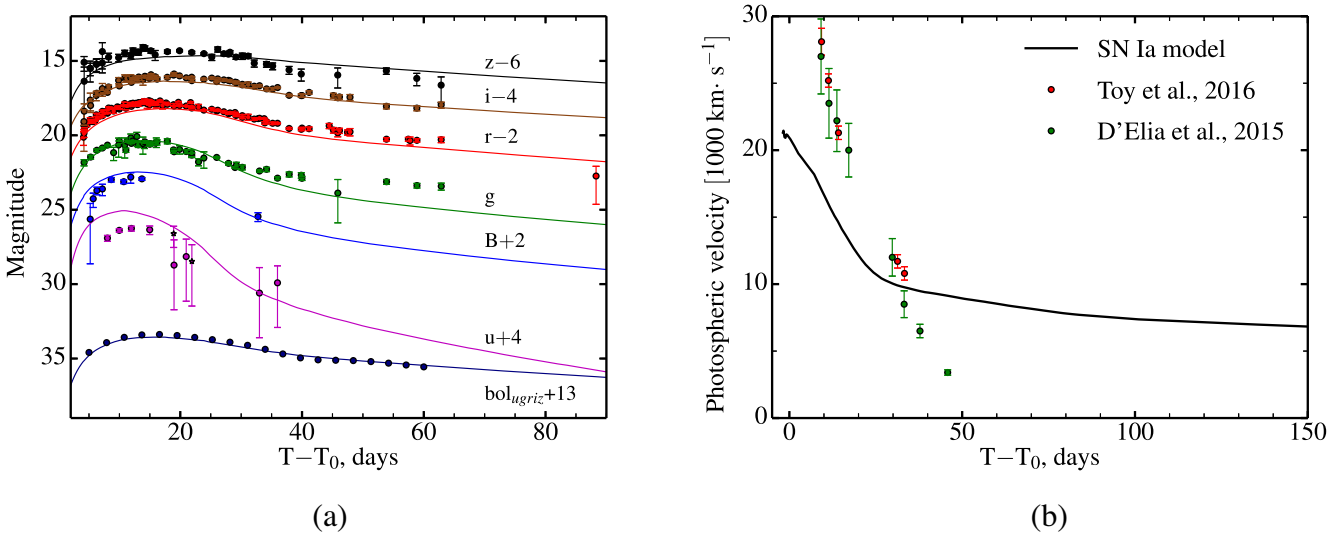

Figure 9. (a) The observed light curve of SN 2013dx (points) and the result of modelling with SN Ia parameters (solid lines). The quasi-bolometric light curve of the SN in the AB photometric system obtained as a sum of the fluxes in the *ugriz* filters is marked as bol$_{ugriz}$. (b) Corresponding photospheric velocities: observed (points) and obtained from the model (solid line).

or to X-ray radiation from the SN component. If this enhancement is related to the SN component, the corresponding luminosity is 4 orders higher than the X-ray luminosity of the well-known SN 1993J (SN IIb, Chandra et al. 2009). However, some GRB-SNe discussed in the literature (e.g. Li & Pun 2011) have X-ray luminosities of GRB-SNe events comparable with our estimates.

5.4 SN energy budget

In Section 4, we derived the total energy of the SN explosion $E_{\rm oburst} = 3.5 \times 10^{52}$ erg and the bolometric energy of the SN radiation from the far-IR to the extreme UV $E_{\rm bol} = 3.1 \times 10^{49}$ erg. We would like to estimate the radiative efficiency of the SN $\eta = E_{\rm rad}/E_{\rm oburst}$, where $E_{\rm rad}$ is the amount of energy released as radiation in both the optical range and X-rays, $E_{\rm rad} = E_{\rm bol} + E_{X,\rm SN}$. If the enhancement of the X-ray flux in the period 5–15 d after the trigger is related to the SN activity (see Section 5.3), we estimate the energy of the SN released in the X-ray domain as $E_{X,\rm SN} = 1.3 \times 10^{49}$ erg. Compiling all these values, the radiative efficiency of the SN explosion is $\eta > 0.1$ per cent. Otherwise, if the SN X-ray emission is negligible, then we obtain a conservative lower limit of the efficiency $\eta \geq 0.08$ per cent.

5.5 Comparison with other GRB-SNe

In our model, we obtained the pre-SN star mass $M = 25\,{\rm M}_\odot$ and the mass of the resulting compact remnant $M_{\rm CR} = 6\,{\rm M}_\odot$. Hence, the total mass of the ejecta is $M_{\rm ej} = 19\,{\rm M}_\odot$. The large ejecta mass and the possible presence of clumps of matter around the progenitor (the bump in red filters) are consistent with the explosion of a rather massive star and suggest that the progenitor of SN 2013dx was a massive Wolf–Rayet star, whose strong winds drove the stripping of the outer layers. A higher ejecta mass is predicted for some Type Ic SNe from a massive progenitor (e.g. SN 2011bm, Valenti et al. 2012). The final mass of the black hole is compatible with current observations and theoretical predictions (see fig. 20 of Sukhbold et al. 2016). However, the ejecta mass is greater than that obtained by D15 and T16, and also greater than the ejecta masses of other GRB-SNe collected by T16 and by Cano et al. (2016, see table 1 there). In contrast, the mass of synthesized nickel $M_{^{56}\rm Ni}$ is lower than that averaged by all GRB-SNe and barely falls in the 1σ interval around the average value. The total energy of the explosion $E_{\rm oburst}$ is greater than the average value and falls into the top third of all GRB-SNe.

Milgrom & Usov (2000) proposed a model of an SN-like explosion induced by a GRB in a binary system. The ejecta of a GRB exposes a white dwarf companion and initiates a Type Ia SN explosion, which would lead to SN Ia phenomenon associated with a GRB. Using the STELLA code, we modelled the light curves of SN 2013dx with a SN Ia model ($M_{^{56}\rm Ni} = 0.35\,{\rm M}_\odot$). The resulting light curves fit the data rather well (see Fig. 9), but the photospheric velocities calculated using this model do not correspond to those measured spectroscopically by D15 and T16. Therefore, the SN Ia model should be discarded.

In T16, the main parameters of the SN were obtained using SN 1998bw as a template. However, by assuming those parameters as input for the modelling, we could not obtain good agreement (see Section 4 and Fig. 7). The parameters reported by T16 do not allow us to reproduce the observations with the model. Thus, we suggest that the light curve of SN 1998bw is not a universal template for describing GRBs associated with SNe. For SN 2013dx, the template of SN 2003dh, used in D15, gives better input parameters for the light-curve modelling.

5.6 Remaining questions

The resulting model is the best from all of the models considered. Still there remain some problems to be resolved:

(i) There is a problem with the simultaneous fitting of observational data in all filters. The time position of the maximum in the modelled and observational light curves does not coincide in every observational range, especially the blue filters. There is an option to vary the start time of the outburst T_0, but for good agreement between the model and the data, one needs to choose different T_0 for the blue and red filters. However, this would break the

self-consistency of the model. This problem may be accounted for by the asymmetry of the outburst.

(ii) Though the modelled quasi-bolometric light curve fits the observational data well, the multicolour model does not fit the peak of the SN well in the blue filters. The discrepancy between the observational points in the *B* and *u* filters and the resulting modelled light curves may be explained by additional absorption along the line of sight that is not included in the host extinction. In the *u* filter near the observed maximum, the difference between the observations and the model is $A_u \sim 1^{\rm m}$, which corresponds to $A_V \sim 0\overset{\rm m}{.}3$ to $0\overset{\rm m}{.}4$ depending on the adopted extinction law. Assuming a wind-like medium and the normalization density parameter A_* from Singer et al. (2013b) (see Section 2.3), we estimated the hydrogen column density $N_{\rm H}$ in the host galaxy of the source by integrating the profile from the radius of the pre-SN star $R = 100\,{\rm R}_\odot$ to infinity. We obtained $N_{\rm H} = 3.7 \times 10^{19}$ cm^{-2}. Assuming the relation between $N_{\rm H}$ and A_V proposed by Güver & Özel (2009) for the Milky Way, we estimate the extinction along the line of sight to be $A_V^{\rm LOS} \sim 0.02^{\rm m}$. This estimation does not allow us to explain the significant difference between the modelled and the observed light curves in the blue filters by some extra extinction along the line of sight or in the host galaxy.

(iii) The resulting model does not describe the secondary bump observed during the SN decay phase, which is clearly visible in the red filters (see Fig. 6). The bump may be connected not with the SN, but with the afterglow. In this case, it may be explained as an interaction of the ejecta with some inhomogeneities in the surrounding interstellar medium, e.g. dense interstellar clouds. A theoretical model proposed by Bisnovatyj-Kogan & Timokhin (1997) considers the prompt gamma-ray emission re-radiating on some dense shell or cloud in the medium surrounding the burst progenitor to form bumps on the light curve. Moreover, there are a few papers with numerical simulations (Postnov et al. 2004; Barkov & Bisnovatyi-Kogan 2005; Badjin, Blinnikov & Postnov 2013). A model of a thick shell or cloud predicts the chromatic behaviour of the bump, i.e. the bluer the filter the earlier the bump, and that the relative brightness in the bluer filters should be more pronounced than in the red ones. Our observations clearly support the prediction of chromatic behaviour, but the flux of the observed bump does not agree with the prediction: on the light curves (Fig. 6a), we clearly see the bump in the *z* filter, while there is no bump in the *g* filter. However, this may be explained by a sparse sampling of the light curve in the *g* filter. Moreover, explaining the bump requires a specific configuration, in particular, there should be a compact dense cloud off-axis to the observer, but not too far to be within the emission cone. The duration of the bump ($\tau_{\rm bump} \sim 10$ d) is explained in numerical simulations with the STELLA code (Badjin et al. 2013).

Similar bumps are present on the light curves of other Type Ib/c SNe, like SN 2003dh associated with GRB 030329, but in this case it is difficult to distinguish the behaviour of the SN light curve from that of the extremely non-monotonic afterglow (see, e.g. Lipkin et al. 2004; Cano et al. 2016, and references therein). There is the potential in the STELLA calculations to take into account the additional interaction of the SN ejecta with the interstellar medium by surrounding the star with a shell (or super-wind), which could induce the bumps on the modelled light curve (Sorokina et al. 2016). We did not implement a super-wind in the current modelling. However, the bump has appeared in some other models in which ^{56}Ni is put in the centre of the explosion without mixing. The absence of the bump on the optimal resulting modelled light curve (Fig. 6a) may be also connected to the simplicity of the assumptions that underlie the model and the code itself.

It is unlikely that the late bump is related to the central engine activity, and thus, to the afterglow evolution. This bump could be related to the re-radiation of the prompt gamma-ray emission by a clumpy circumburst medium, but in this case one would expect to observe several bumps from the interaction of the gamma-rays with every clump around the source (e.g. the late light curve of GRB 030329; Lipkin et al. 2004). The observed bump could be natural if the circumburst medium consisted of only one single clump. We cannot definitely determine the bump's nature and we suggest that it is related to the SN. Similar bumps may emerge in models with a different ^{56}Ni distribution inside a pre-SN star (Moriya et al. 2016, see also Figs 8b, c and d).

6 CONCLUSIONS

The light curve of SN 2013dx associated with GRB 130702A is the second-best sampled GRB-SN after SN 1998bw. We collected all the available optical data of this event: the multicolour light curves of GRB 130702A contain 330 data points in filters *uBgrRiz* until 88 d after the burst start, and more than 280 of them form the light curves of the associated supernova SN 2013dx. 40 of these points are published for the first time.

We presented the multicolour light curves of this SN, modelled with the code STELLA. In general, the model for the filters as well as the quasi-bolometric light curve are in fairly good agreement with the observations. Moreover, the STELLA predictions of the photospheric velocities fit those obtained from the spectra well. The bolometric parameters of the SN according to the model are: $M = 25\,{\rm M}_\odot$, $M_{\rm CR} = 6\,{\rm M}_\odot$, $E_{\rm oburst} = 3.5 \times 10^{52}$ erg, $R = 100\,{\rm R}_\odot$, $M_{^{56}{\rm Ni}} = 0.2\,{\rm M}_\odot$ (and the Ni is totally mixed inside the envelope), $M_{\rm O} = 16.6\,{\rm M}_\odot$, $M_{\rm Si} = 1.2\,{\rm M}_\odot$ and $M_{\rm Fe} = 1.2\,{\rm M}_\odot$.

Disagreement between the modelled flux and the data increases from the red to the blue filter (from *g* to *u*). Comparison between the model and the data at the peak of the light curve suggests evidence for an additional line-of-sight extinction in the host galaxy, but the presence of this additional extinction is not confirmed by other methods of investigation, namely, by modelling the host SED and circumburst environment density. Instead, it might be related with a non-homogeneous mixing of ^{56}Ni.

The modelling of the SN light curve allowed us to estimate the conversion factor between the total energy of the SN outburst and the energy emitted by the SN as electromagnetic radiation to be 0.1 per cent.

GRB 130702A is one more GRB with extended emission detected in the gamma-ray light curve. Since the central engine is thought to power the extended emission, this might suggest that GRB 130702A's central engine is similar to those of GRB 111209A and GRB 130831A.

ACKNOWLEDGEMENTS

We are grateful to M. Barkov, S. Grebenev, S. Moiseenko, B. Fain and V. Loznikov for useful discussions. We are thankful for the anonymous referee for valuable remarks. The work of AAV, ASP, PYuM and EDM (data reduction, analysis, interpretation and comparison with other GRB-SNe) was supported by Russian Science Foundation grant 15-12-30016. MVP acknowledges support from Russian Science Foundation grant 14-12-00146 for SN modelling with the STELLA code. The work of SIB (development of the STELLA code) was supported by Russian Science Foundation grant 14-12-00203. Grant IZ73Z0_152485 SCOPES Swiss National Science

Foundation supports the work of SIB on the production of radioactive elements in stellar explosions. The work at Abastumani was supported by the Shota Rustaveli National Science Foundation, grant FR/379/6-300/14. All observations at Maidanak Astronomical Observatory were supported by a grant from the Committee for Coordination Science and Technology Development of Uzbekistan (F2-AS-F026). We gratefully acknowledge observers B. Khafizov and O. Parmonov for support of observations at Maidanak Astronomical Observatory. OAB is thankful to the Matsumai International Foundation (MIF, Tokyo, Japan) (research fellowship 15G24). This work made use of data supplied by the UK Swift Science Data Centre at the University of Leicester. This research has made use of NASA's Astrophysics Data System.

REFERENCES

Amati L. et al., 2002, A&A, 390, 81
Amati L., Dichiara S., Frontera F., Guidorzi C., Izzo L., Della Valle M., 2013, GCN Circulars, 15025
Arnett W. D., 1982, ApJ, 253, 785.
Arnouts S., Cristiani S., Moscardini L., Matarrese S., Lucchin F., Fontana A., Giallongo E., 1999, MNRAS, 310, 540
Atwood W. B. et al., 2009, ApJ, 697, 1071
Badjin D. A., Blinnikov S. I., Postnov K. A., 2013, MNRAS, 432, 2454
Baklanov P. V., Blinnikov S. I., Pavlyuk N. N., 2005, Astron. Lett., 31, 429
Band D. L., 1997, ApJ, 486, 928
Band D. et al., 1993, ApJ, 413, 281
Barkov M. V., Bisnovatyi-Kogan G. S., 2005, Astron. Rep., 49, 24
Barkov M. V., Pozanenko A. S., 2011, MNRAS, 417, 2161
Bennett C. L., Larson D., Weiland J. L., Hinshaw G., 2014, ApJ, 794, 135
Beuermann K. et al., 1999, A&A, 352, L26
Bisnovatyj-Kogan G. S., Timokhin A. N., 1997, Astron. Rep., 41, 423
Blanton M. R., Roweis S., 2007, AJ, 133, 734
Blinnikov S. I., Eastman R., Bartunov O. S., Popolitov V. A., Woosley S. E., 1998, ApJ, 496, 454
Blinnikov S. I., Röpke F. K., Sorokina E. I., Gieseler M., Reinecke M., Travaglio C., Hillebrandt W., Stritzinger M., 2006, A&A, 453, 229
Bufano F., Benetti S., Sollerman J., Pian E., Cupani G., 2011, Astron. Nachr., 332, 262
Burrows D. N. et al., 2005, Space Sci. Rev., 120, 165
Cano Z., 2013, MNRAS, 434, 1098
Cano Z. et al., 2014, A&A, 568, A19
Cano Z., Wang S.-Q., Dai Z.-G., Wu X.-F., 2016, preprint (arXiv:1604.03549)
Cenko S. B., Gal-Yam A., Kasliwal M. M., Stern D., Markey K., Alduena E., Alduena A., Kuo S., 2013. GCN Circulars, 14998
Chandra P., Dwarkadas V. V., Ray A., Immler S., Pooley D., 2009, ApJ, 699, 388
Cheung T., Vianello G., Zhu S., Racusin J., Connaughton V., Carpenter B., 2013, GCN Circulars, 14971
Chugai N. N. et al., 2004, MNRAS, 352, 1213
Collazzi A. C., Connaughton V., 2013, GCN Circulars, 14972
Corsi A., Perley D. A., Cenko S. B., 2013, GCN Circulars, 14990
D'Avanzo P., D'Elia V., Tagliaferri G., Melandri A., Malesani D., Della Valle M., Pian E., 2013a. GCN Circulars, 14984
D'Avanzo P., Porterfield B., Burrows D. N., Siegel M., Melandri A., Evans P. A., 2013b, GCN Circulars, 14973
D'Elia V. et al., 2013, GCN Circulars, 15000
D'Elia V. et al., 2015, A&A, 577, A116 (D15)
De Pasquale M. et al., 2016, MNRAS, 455, 1027
Evans P. A. et al., 2009, MNRAS, 397, 1177
Ferrero P., Palazzi E., Pian E., Savaglio S., 2007, in di Salvo T., Israel G. L., Piersant L., Burderi L., Matt G., Tornambe A., Menna M. T., eds, AIP Conf. Ser. Vol. 924, The Multicolored Landscape of Compact Objects and Their Explosive Origins. Am. Inst. Phys., New York, p. 120
Filippenko A. V., 1997, ARA&A, 35, 309
Fioc M., Rocca-Volmerange B., 1997, A&A, 326, 950
Folatelli G. et al., 2006, ApJ, 641, 1039
Galama T. J. et al., 1998, Nature, 395, 670
Gehrels N., 2004, ApJ, 611, 1005
Golenetskii S., Aptekar R., Pal'Shin V., Frederiks D., Oleynik P., Ulanov M., Svinkin D., Cline T., 2013, GCN Circulars, 14986
Gruber D. et al., 2014, ApJS, 211, 12
Güver T., Özel F., 2009, MNRAS, 400, 2050
Hjorth J., Bloom J. S., 2012, The Gamma-Ray Burst – Supernova Connection. Cambridge Univ. Press, Cambridge, p. 169
Hurley K. et al., 2013. GCN Circulars, 14974
Ilbert O., 2006, A&A, 457, 841
Ishida E. E. O., de Souza R. S., 2013, MNRAS, 430, 509
Ishida E. E. O., Abdalla F. B., de Souza R. S., 2014, in Heavens A. F., Starck J.-L., Krone-Martins A., eds, Proc. IAU Symp. 306, Statistical Challenges in 21st Century Cosmology. Kluwer, Dordrecht, p. 326
Iwamoto K. et al., 1998, Nature, 395, 672
Kelly P. L., Filippenko A. V., Fox O. D., Zheng W., Clubb K. I., 2013, ApJ, 775, L5
Komissarov S. S., Barkov M. V., 2009, MNRAS, 397, 1153
Kouveliotou C., Meegan C. A., Fishman G. J., Bhat N. P., Briggs M. S., Koshut T. M., Paciesas W. S., Pendleton G. N., 1993, ApJ, 413, L101
Kozyreva S. et al., 2017, MNRAS, 464, 2854
Kromer M., Sim S. A., 2009, MNRAS, 398, 1809
Kulkarni S. R. et al., 1998, Nature, 395, 663
Law N. M. et al., 2009, PASP, 121, 1395
Leloudas G., Fynbo J. P. U., Schulze S., Xu D., Malesani D., Geier S., Cano Z., Jakobsson P., 2013, GCN Circulars, 14983
Li K. L., Pun C. S. J., 2011, preprint (arXiv:1109.0981)
Liang E.-W., Racusin J. L., Zhang B., Zhang B.-B., Burrows D. N., 2008, ApJ, 675, 528
Lipkin Y. M. et al., 2004, ApJ, 606, 381
Lyons N., O'Brien P. T., Zhang B., Willingale R., Troja E., Starling R. L. C., 2010, MNRAS, 402, 705
MacFadyen A. I., Woosley S. E., 1999, ApJ, 524, 262
Markwardt C. B., 2009, in Bohlender D. A., Durand D., Dowler P., eds, ASP Conf. Ser. Vol. 411, Astronomical Data Analysis Software and Systems XVIII. Astron. Soc. Pac., San Francisco, p. 251
Mazzali P. A. et al., 2003, ApJ, 599, L95
Meegan. C. et al., 2009. ApJ, 702, 791
Milgrom M, Usov V. V., 2000, ApJ, 531, L127
Moriya T. J., Pruzhinskaya M. V., Ergon M., Blinnikov S. I., 2016, MNRAS, 455, 423
Mulchaey J., Kasliwal M. M., Arcavi I., Bellm E., Kelson D., 2013a, GCN Circulars, 14985
Mulchaey J., Kasliwal M. M., Arcavi I., Bellm E., Kelson D., 2013b, Astron. Telegram, 5191
Norris J. P., 2002, ApJ, 579, 386
Norris J. P., Bonnell J. T., Kazanas D., Scargle J. D., Hakkila J., Giblin T. W., 2005, ApJ, 627, 324
Pačiesas W. S., 2004, Balt. Astron., 13, 187
Perley D., Kasliwal M., 2013, GCN Circulars, 14979
Perley D. A. et al., 2014, ApJ, 781, 37
Postnov K. A., Blinnikov S. I., Kosenko D. I., Sorokina E. I., 2004, Nuclear Phys. B Proc. Suppl., 132, 327
Pozanenko A., Volnova A., Burhonov O., Molotov I., 2013, GCN Circulars, 14988
Prévot M. L., Lequeux J., Prevot L., Maurice E., Rocca-Volmerange B., 1984, A&A, 132, 389
Rau A. et al., 2009, PASP, 121, 1334
Sari R., Piran T., Narayan R., 1998, ApJ, 497, L17
Schlafly E. F., Finkbeiner D. P., 2011, ApJ, 737, 103
Schulze S., Leloudas G., Xu D., Fynbo J. P. U., Geier S., Jakobsson P., 2013, GCN Circulars, 14994
Sim S. A., Kromer M., RŁopke F. K., Sorokina E. I., Blinnikov S. I., Kasen D., Hillebrandt W., 2010, in Pogorelov N. V., Audit E., Zank G. P., eds, ASP Conf. Ser., Numerical Modeling of Space Plasma Flows. Astron. Soc. Pac., San Francisco, p. 148

Singer L. P. et al., 2013a, GCN Circulars, 14967
Singer L. P. et al., 2013b, ApJ, 776, L34
Sorokina E., Blinnikov S., Nomoto K., Quimby R., Tolstov A., 2016, ApJ, 829, 17
Sukhbold T., Ertl T., Woosley S. E., Brown J. M., Janka H.-T., 2016, ApJ, 821, 38
Tauris T. M., Langer N., Moriya T. J., Podsiadlowski Ph., Yoon S.-C., Blinnikov S. I., 2013, ApJ, 778, 23
Tominaga N., Blinnikov S., Baklanov P., Morokuma T., Nomoto K., Suzuki T., 2009, ApJ, 705, 10
Toy V. L. et al., 2016, ApJ, 818, 79 (T16)
Valenti S., 2012, ApJ, 749, L28
van der Horst A. J., 2013, GCN Circulars, 14987
Vietri M., Stella L., 1998, ApJ, 507, L45
Woosley S. E., Kasen D., Blinnikov S., Sorokina E., 2007, ApJ, 662, 487
Wright E. L., 2006, PASP, 118, 1711
Zhang B. et al., 2007, ApJ, 655, 989

This paper has been typeset from a TEX/LATEX file prepared by the author.